The unlocking process of the 2016 Central Italy seismic sequence

Sugan M.[1], Campanella S.[1], Chiaraluce L.[2], Michele M.[2], Vuan A.[1]

[1] National Institute of Oceanography and Applied Geophysics – OGS (Italy)

[2] Istituto Nazionale di Geofisica e Vulcanologia (Italy)

Corresponding author: Monica Sugan (msugan@ogs.it)

Key Points:

- 8-years seismic data scrutinized by template matching provide ~5 times more events before the M_w 6.0 Amatrice mainshock
- fore-mainshocks and swarm-like clusters persisted before the Amatrice main at the northern and southern fault edges of the nucleation point
- an unlocking process by progressive deformation localization weakened the 2016 main fault volume peripheral area

Abstract

Approximately 23,000 well-located earthquakes from 2009 to 2016 are used as templates to recover seismic activity preceding the 2016 Central Italy seismic sequence. The resulting spatiotemporal pattern is analyzed employing ~91,000 newly detected events. In the 8 years before the sequence onset, microseismicity ($M_L \leq 3.7$) develops at the hangingwall of the 2016 fault system and along a sub-horizontal shear zone. The events, mainly organized in clusters, represented by foreshock-mainshock and swarm-like sequences, migrate toward the nucleation area of the first M_w 6.0 mainshock of the sequence that occurred on the 24th of August in Amatrice. We propose an unlocking model based on variable temporal clustering of the seismicity, including repeaters, identifying fault portions with different degree of coupling and rheology, responding differently to the tectonic loading, and working to progressively localize the deformation process, increasing rock damage and weakening the nucleation patch of the Amatrice mainshock.

Keywords: template matching, unlocking, swarms, foreshocks, slow slip, progressive deformation

Plain Language Summary

We exploit a high-resolution earthquakes catalog to describe the seismic activity preceding the cascade-like 2016 Central Italy seismic sequence. Newly retrieved events are analyzed in space and time to characterize the earthquake preparatory phase leading to the first mainshock of the sequence.

Our 8-years-long observations show rock damage related to seismic activity involving structures surrounding the nucleation and rupture zone. Intriguing seismicity patterns along an almost horizontal discontinuity below the normal faults and at their northern and southern edges are found. We highlight migrations, clustering, and progressive deformation localization close to the first mainshock of the sequence, unveiling a complex preparatory phase.

1. Introduction

In the last 25 years, the central Apennines have been the site of moderate-strong ($5.9 <= M_w <= 6.5$) extensional earthquakes (Colfiorito 1997; L'Aquila 2009; Central Italy 2016). Contrary to what happened in both 1997 (Ripepe et al., 2000) and 2009 (Lucente et al., 2010) crises, the 2016 sequence initiated without conventional foreshocks activity.

The sequence evolved around its largest event (M_w 6.5, 30th October) near Norcia, located in the middle of a fault system activated two months earlier, with a first M_w 6.0 (24th August) event located south, near the town of Amatrice. Then, a few days before the Norcia earthquake, another M_w 5.9 event occurred at the northernmost extent of the sequence, near the village of Visso (Figure 1).

Aftershocks distribution clearly shows the geometry of the shallow SW-dipping normal fault segments hosting the mainshocks of the sequence, confined at depth by a sub-horizontal about 2-3 km thick shear zone active between 7-12 km (SZ; Chiaraluce et al., 2017, Waldhauser et al., 2021); a discontinuity interpreted as a litho-structural feature or as the limit of the brittle-ductile transition, contributing to pre- co- and post-seismic displacement (Barchi et al., 2021; Mandler et al., 2021).

Before the M_w 6.0 Amatrice mainshock, seismicity rate changes along the SZ (Vuan et al., 2017) and pre-slip (Vičič et al., 2020), linked to supposed temporal fluctuations in tectonic loading, are observed close to the system of shallow dipping normal faults. In the eight months preceding the 2016 sequence onset, seismic activity increased along the SZ in the areas located at the termination of the normal faults that will host the strongest earthquakes. These time-varying rates have been interpreted as the brittle signature of the tectonic loading process acting along the normal fault's bounding plane, suggesting an active role of the SZ in the preparatory earthquake phase (Vuan et al., 2017). Tan et al. (2021) and Waldhauser et al. (2021) observed that during the aftershock sequence, the SZ seismicity mainly occurs in response to the slip on the normal faults, proposing a different and passive role for this structure during the coseismic stage.

All these findings highlight SZ's time-dependent and evolving behavior during the preparatory process and in the co- and post-seismic phase. Thus, to constrain the driving process leading to the unlocking mechanisms of the 2016 seismic sequence and to better interpret the relationships between high angle normal faults and the sub-horizontal shear zone, we increase the spatio-temporal resolution of the seismicity patterns by using a template matching approach (Vuan et al., 2018; 2020 Sugan et al., 2014; 2019).

To look for previously undetected events contained within ~8 years of continuous data, we use a catalog of approximately 23,000 well-relocated earthquakes that occurred within the source volume containing the 2016-17 Central Italy sequence and were detected by the Italian National Network from the 1st of January 2009 and the 24th of August 2016, the day of the Amatrice mainshock (Figure 1).

The augmented catalog is used to identify areas with different frictional properties by investigating and defining the typology of clustering (e.g., foreshock-mainshock, typical mainshock-aftershock, or swarm-like; Zaliapin and Ben-Zion 2016 and 2020) over time and space.

Within the clusters characterized by higher waveforms similarity, we look for repeating earthquakes to be possibly associated with the occurrence of aseismic slip, such as creeping, afterslip, or slow slip events (e.g., Uchida, 2019).

These features are then discussed together to define the earthquake preparatory phase and nucleation process in the framework of published models (Ellsworth et al., 2018, Tape et al., 2018, Kato and Ben-Zion, 2021).

2. Methods

2.1 Input catalog

The catalog of templates consists of 23,003 events in the local magnitude (M_L) range 0.1 – 5.2 that occurred in the 100 x 100 km^2 area shown in Figure 1 from the 1^{st} of January 2009 to the onset of the 2016 Central Italy sequence (24^{th} of August 2016). The events have been initially relocated in absolute terms using NonLinLoc code (Lomax et al., 2000), based on a nonlinear inversion method (Figure S1 in the supplement).

To further maximize the quality of the templates' catalog in terms of hypocentral location resolution, we apply a double difference (Waldhauser and Ellsworth, 2000) scheme taking only absolute travel times. The resulting relocations show the mean value of horizontal errors of ~500 m in an east-west direction and ~400 m north-south. The mean value of vertical errors is ~400 m, as reported in Figure S2 in the supplementary material. Details about the methods are described in supplement Text S1**.**

2.2 Template matching

Template matching (Vuan et al., 2018) is applied to 8-years continuous data recorded before the 2016 Central Italy sequence, placed between Colfiorito 1997 and L'Aquila 2009, to gain greater detail in microseismicity patterns, possibly inferring indications of the earthquake preparation phase.

Text S2 in the supplement describes the method and input and output parameters to infer and validate the augmented catalog.

We keep the new detections co-located with the templates, while the magnitude is estimated by amplitude comparison with the templates. A tenfold increase in the amplitude ratio corresponds to a one-unit increase in magnitude at each recording channel.

2.3 Clustering analysis and repeating earthquakes

We analyze the clustering of the events in the augmented catalog over time and space (see **Text S3** in the supplement) by applying the Zaliapin and Ben-Zion (2016, 2020) approach that separates the clusters from the background seismicity. Subsequently, we define and classify the clusters as swarms, mainshock-aftershock, and foreshock-mainshock sequences, following the criterion proposed by Ogata and Katsura, 2012.

We also investigated temporal clustering (covariance of interevent times; Kagan and Jackson, 1991) and seismic moment ratio evolution over time (Vidale and Shearer,

1996) to define the level of complexity, fault interactions, volumetric processes, and heterogeneous fault properties. The interevent-time statistics method does not rely on any triggering mechanism or declustering algorithm (Liu et al., 2022). We also explore the mechanical properties of the activated faults and surrounding regions by focusing on the presence of repeating earthquakes. In particular, we adopt a method that combines both seismic waveform similarity, using a cross-correlation function and differential S-P travel time measured at each seismic station (Shakibay Senobari and Funning 2019; Sugan et al., 2022). Details about the parameters and the approach adopted to declare repeating earthquakes are provided in the supplementary material (**Text S4** in the supplement).

3. Results

In the 8-years preceding the Amatrice earthquake, template matching helped detect approximately 91,000 new events (**Catalog_TM** in supplementary), lowering the magnitude of completeness (M_C) of the augmented catalog by about 1 degree of magnitude, reaching M_C = 0.4. The ability of the templates to find new events spans homogenously over time, including events with a high degree of waveform similarity (cross-correlation values >0.9; Figure S3).

The templates, located in a square area of approximately 10,000 km^2, identify persistent microseismic activity from 2009 to 2016 in key sectors of the complex system of faults activated later during the Central Italy sequence. Most seismicity is located below 7 km, while the 2016 main sequence spreads a broader range, including the shallower crustal volume (<7km; Figure S4).

We analyze the pre-sequence augmented catalog divided above and below the SZ. By applying a tuned ridge estimator of the scattered seismicity (Amini and Roozbeh, 2015), we identify a smooth 3D surface at the top of the SZ (TSZ; Figure S5). The definition of the top of the SZ seismicity at variable depths is possible because of the presence of a thin layer (~ 1 km) showing less microseismicity (Vuan et al., 2017) and partially separating the shallow extensional fault system activated during the sequence from the underlying shear zone seismicity.

The TSZ east-dipping boundary is more evident below and north of the 2016 fault system, while in the southern sector, it mixes up in terms of both seismic activity (e.g., aftershocks) and geometry with the deeper and low angle portion of the Campotosto fault, activated with a series of $5<M_W<6$ events during the 2009 L'Aquila sequence (Valoroso et al., 2013).

TSZ depth values range from 7 to 12 km and do not differ significantly from the TSZ roughly reconstructed in Vuan et al. (2017).

A space and time representation of the eight-year augmented catalog and the corresponding yearly frequency of events are shown in Figure 2. Seismicity is projected along the 2016 main faults mean strike (336 degrees – N24W) with positive and negative offset values toward the north and south of the 24th of August Amatrice mainshock nucleation point. Figure 2 highlights two main features: the lack of activity right below the Amatrice fault (below the TSZ; Figure 2d) and the migration in time of the shallower (above the TSZ) seismic activity toward the Amatrice fault zone (Figure 2b).

Although remaining active during the 8-years time window, the SZ concentrates the events north and south of the Amatrice main fault edge (Figures 2c). Below this fault volume, a lower seismicity rate is found. On the contrary, the SZ becomes very active after each mainshock of the 2016 sequence (Tan et al., 2021; Waldhauser et al., 2021; Barchi et al., 2021). The clustering of events above the SZ migrates from south to north, progressively affecting the main fault volume from 2013 (Figure 2b).

The period from 2009 to the end of 2011 is characterized by a concentration of events in the Campotosto area (south of the 2016 main fault: Figure 2a), both above and below the TSZ. This is caused by the still ongoing aftershocks activity of the 2009 L'Aquila sequence extended in time, presumably due to the triggering effect of the pore pressure diffusion process described by Malagnini et al. (2021). After 2013, we still observe activity in the southern part of the Amatrice fault, in the Campotosto area, even if the number of events decreases.

Clusters above the TSZ inside the Amatrice fault volume are observed starting from 2013 (Figures 2a, b). At the same time, diffused seismicity is also active close to the northern fault edge within the SZ (Figure 2c, d). From the second half of 2015 until the sequence onset (with the Amatrice M_W 6.0 mainshock on the 24th of August 2016), clusters are found within the main fault volume and close to the Amatrice nucleation point.

We apply a space-time nearest-neighbor technique (Zaliapin and Ben-Zion 2016, 2020) to distinguish better clustered from background activity (Figure 3), plus a frequency-magnitude distribution criterion (Ogata and Katsura 2012) for classifying the identified clusters as swarm-like, foreshock-mainshock, and mainshocks.

Within our 8-years long catalog, we identify approximately 670 clusters (number of events higher than 10) lasting from days to months and a maximum magnitude generally lower than M_L 3 (Figure S4). Clusters constitute 51% of the total seismicity and are mainly foreshock-mainshock (22%) or swarm-like sequences (28%). Few clusters classified as swarms revealed a mixed behavior with bursts' repetitions in a few days.

Figures 3a and 3b help distinguish areas with different clustering or diffuse seismicity above and below TSZ. Above the TSZ (Figure 3a), clusters are mainly found in the hanging wall of the fault system and predominate in the southern sector (S) or within the fault volume (F). The northern sector (N) is characterized by a few clusters at the edges and a low background seismicity rate. Below the TSZ (Figure 3b), swarms and fore-mainshock sequences are more abundant in the S sector. The N and F sectors show very few clusters but with, respectively, a higher and meager background seismicity rate.

The along-strike projection of the clusters and background seismicity versus time, above and below the TSZ, is shown in Figures 3c and d, respectively. Figures 3c,d reflect what is described in Figure 2. Above the TSZ, clusters migrate from N and S toward the F sector, decreasing one year before the mainshock. Clusters below the TSZ evolve differently: we find swarm-like sequences in the S sector up to 2015 and in the footwall out of the N sector, while few foreshock-mainshock clusters develop within and around the F sector.

We also find repeating earthquakes, doublets characterized by low interevent time (generally less one day), following the same migration shown by the other clusters above TSZ (Figure 3c) toward the nucleation point of the 24th August Amatrice mainshock. Some are also found below the TSZ, close to the Campotosto area, and north of the Amatrice fault (Figure 3d).

To better investigate the difference in the mechanical properties of the faults system, we use clustering as a proxy for identifying areas and periods of different coupling and frictional properties. Generally, weaker temporal clustering characterizes creeping volumes where the coupling in the main fault volume is lower (Liu et al., 2022). Differently, locked volumes with higher coupling show a more pronounced temporal clustering.

The covariance of interevent times (Figs. 4a, b), the seismic moment ratio (Figs. 4c, d), and the cumulative rate over time (Fig. 4e, f) are computed for the volume hosting the fault (area F in Figure 3) and for the N and S sectors of Figure 3 (Figures S6 and S7) to evaluate the degree of coupling above and below the TSZ.

Low and high covariance values are often alternated in F. At the same time, an evident increase in temporal clustering was found in 2013 when the activity above the TSZ changed from Poissonian to clustered (Fig. 4a), while below the TSZ (Fig. 4b), unclustered diffuse seismicity prevails.

The moment ratio is generally low after 2013 (Figure 4c and 4d), indicating clustered swarm-like sequences, often observed elsewhere during increased over-pressurized fluids in fault volumes (Zhu et al., 2020). In general, moment ratios between 0.5 and 1 evidence fore-mainshock coexisting with swarms-like clusters.

The cumulative number of events is higher above the TZS than below (Figures 4e and f). In the shallower crust from 2013, the high temporal clustering suggests high coupling, while diffuse low-level seismicity is found below TZS.

In the north-northwestern sector (N), covariance values above the TSZ show few clusters (Figure S6a), less than in the F sector (Fig. 4a). From 2012 to 2013, below the TSZ, seismicity appears to be more diffuse than in F, with no apparent temporal clustering and Poissonian (Figure S6b). In N, moment ratios slightly increase from 2012 (Figure S6c). Despite the higher density of events below the TSZ than above (Figure S6d), moment ratios are lower than 0.5. The weaker temporal clustering suggests low coupling for N.

South of the main fault volume (Campotosto area, S in Figure 3a), a relatively low covariance value is observed above TZS up to 2011. Subsequently, the values rise for some clusters starting from the second half of 2011 (Figure S7a). Moderate covariance values are also found from 2015 to 2016 below TSZ (Figure S7b).

The moment ratio shows prevailing mainshock-aftershock and foreshock-mainshock sequences up to mid-2011, followed by predominant swarm-like clusters and foreshock-mainshock (Figure S7c and d). The high cumulative number of events that characterizes this sector from 2009 to mid-2011 is still related to the L'Aquila 2009 aftershock sequence.

4. Discussion

In the 8-years before the first Mw 6.0 Amatrice mainshock of the 2016 sequence, seismicity highlighted by the newly retrieved catalog appears to mainly occur along a shear zone (SZ) located below ~7 km and bounding at depth the normal faults system.

The seismicity pattern (Figure 2) shows that the seismic release along the SZ is relatively constant and unclustered, with a release rate lower at the base of the Amatrice mainshock fault than in the surrounding areas.

On the contrary, above the SZ, within the shallower crustal volume hosting the main normal fault where the mainshocks nucleate, we observe seismic activity organized in clusters (mainly foreshocks-mainshock and swarms) nucleating around the main fault zone (Figure 3), together with repeating earthquakes and producing progressive rock damage migrating in time toward the Amatrice nucleation area (Figures 3). The migration pattern observed at shallow depth from the southern portion to the fault volume and repeating earthquakes can be interpreted as an aseismic slip process.

Similarly, Vičič et al. (2020), using GPS data preceding the mainshock, suggest that aseismic deformation plays a fundamental role in loading surface faults.

Observations of aseismic transients in the shallow crust are less common than in subduction zones because it is hypothesized that slow slip requires a rich content of over-pressurized fluids and higher temperatures not often found in the colder, drier continental crust (Bouchon et al., 2013). Over-pressurized fluids (CO_2) are well documented along in this sector of the Apennines, being encountered at around 5-6 km of depth in a few deep boreholes drilled for oil investigation activities (Trippetta et al., 2013; Chiodini et al., 2013; Lombardi et al., 2010). Thus, fluid-driven slow slip can be possible in an extensional framework showing clustered activity with the presence of foreshocks and progressive localization of deformation.

More recently, Malagnini et al. (2022) measured time variations of seismic attenuation, a parameter strongly linked to crustal permeability, and interpreted the 2016 Central Italy sequence as an extended episode of fluid diffusion. Coseismic permeability changes evidenced by seismic attenuation are responsible for creating fluid diffusion pathways enabling the triggering of multi-mainshocks.

Abundant fluids in Central Italy are also supposed by the presence of migrating swarm-like clusters. Ross and Cochran (2021) interpreted swarms as an effect of transient natural fluid injection processes in southern California. Thus, the final preparation phase leading to large earthquakes could be driven by a mixture of slow-slip transients and fluids.

Tiny slow slip seismic transients could contribute to the build-up of shear stress on mainshock hypocenter sites and stress changes induced by foreshock ruptures. When a strong small patch on a fault breaks, it rapidly increases the patch's loading rate, making the surrounding fault more brittle and susceptible to dynamic rupture (Kato and Ben-Zion 2021). In 2013 within the fault volume, as described in Figures 3 and 4a, we observed an intermittent, step-like fault slip behavior with typical swam-like seismic bursts. This intermittent slip could represent a combination of slow and fast failure modes, increasing the stress on the eventual rupture zone and producing local variations in loading rates that modify the effective frictional behavior of the main fault.

Assuming the temporal clustering as a proxy of the main fault volume coupling, we define the existence of a creeping activity along a basal detachment characterized by low coupling, increasing the loading on the above locked high-angle normal faults (higher coupling). We highlight a northwestern creeping region, where diffuse seismicity prevails below the TZS, and a southern region with moderate coupling below TSZ, where fluid diffusion occurs. We provide in Figure S8 a simplified sketch to synthesize our observations and results on the preparation process of the 2016 Central Italy seismic sequence.

Identifying the locked areas of the fault accumulating elastic strain to be released during a future earthquake and areas slowly releasing strain through aseismic creep are essential when examining the nucleation processes. The nucleation of a dynamic rupture is related to the evolution and variations of stress and strength in the fault system volume. The two end-member models describing such a process are the cascade-up (e.g., Ellsworth et al., 2018) and the pre-slip (e.g., Tape et al., 2018). Between these models, there is the progressive deformation localization one (Ben-Zion and Zaliapin, 2020; Kato and Ben-Zion, 2021), which supposes evolving distributed rock damage to localized deformation, leading to a primary slip zone prone to a significant dynamic rupture (e.g., Amitrano et al., 1999; Renard et al., 2019). During the localization, microseismicity monitoring could play a role, and clusters or foreshocks could trace in space and time the evolving process that might lead to the nucleation of the mainshock rupture (Kato and Ben-Zion, 2021).

The described eight-year seismicity patterns find analogs with the model proposed by Kato and Ben-Zion (2021). Before the 2016 central Italy sequence, we observe the generation of rock damage by ongoing seismicity around a future rupture zone producing crustal weakening on a multi-annual scale, background seismicity localization, and coalescence of events into growing clusters in the final ~3–4 years before the large earthquakes.

5. Conclusions

The initiation of major earthquakes results from multiple processes acting at various spatial and temporal scales. The novel and increased catalog we generate, composed of about 91,000 events, highlights a progressive deformation localization before the first M_w 6.0 mainshock of the 2016 Central Italy sequence.

Our 8-years observations show rock damage related to seismic activity involving structures surrounding the nucleation and main rupture zone. The pre-sequence seismicity patterns along the almost horizontal SZ demonstrate an evolution of damage at the base of normal faults at the northern and southern main fault edges that probably triggered clusters and seismicity within the main fault volume. Localization of background seismicity and growing clusters migrating within the main fault volume produce crustal weakening around the future rupture zone, with progressive unlocking. The migrating clusters, mainly formed by foreshocks-mainshocks and swarm-like clusters also including repeating earthquakes, suggest the occurrence of slow slip transients, probably boosted by fluids.

Acknowledgments

This study was supported by the Real-time earthquake rIsk reduction for a reSilient Europe (RISE) project, funded by the European Union's Horizon 2020 research and innovation program under Grant Agreement Number 821115 and partially funded by the Istituto Nazionale di Oceanografia e Geofisica Sperimentale (OGS). Maddalena Michele received financial support from RISE.

The research reported in this work was also supported by OGS and CINECA under HPC-TRES program award number 2021-01. Figures were produced using the Generic Mapping Tools (Wessel and Luis, 2017) version 6.3.0 (http://gmt.soest.hawaii.edu). We thank Ilya Zaliapin for kindly providing the declustering code.

Data Availability Statements

Data used in this article are available via EIDA (the European Integrated Data Archive infrastructure within ORFEUS) at http://www.orfeus-eu.org/webdc3/.

References

Amini, M., & Roozbeh, M. (2015). Optimal partial ridge estimation in restricted semiparametric regression models. *Journal of Multivariate Analysis, 136,* 26–40. https://doi.org/10.1016/j.jmva.2015.01.005.

Amitrano, D., Grasso, J.-R., & Hantz, D. (1999). From diffuse to localized damage through elastic interaction. *Geophys. Res. Lett.,* 26(14), 2109-2112.

Baillard, C., Crawford, W.C., Ballu, V., Hibert, C., & Mangeney, A. (2014). An Automatic Kurtosis-Based P- and S-Phase Picker Designed for Local Seismic Networks. *Bull. Seism. Soc. Am.*, 104(1), 394-409. https://doi.org/10.1785/0120120347.

Barchi, M. R., Carboni, F., Michele, M., Ercoli, M., Giorgetti, C., Porreca, M., Azzaro, S., & Chiaraluce, L. (2021). The influence of subsurface geology on the distribution of earthquakes during the 2016– 2017 Central Italy seismic sequence, *Tectonophysics* 807, 228797. https://doi.org/10.1016/j.tecto.2021.228797.

Ben-Zion, Y., & Zaliapin, I. (2020). Localization and coalescence of seismicity before large earthquakes. *Geophys. J. Int.,* 223(1), 561–583. https://doi.org/10.1093/gji/ggaa315.

Bouchon, M., Durand, V., Marsan, D., Karabulut H., & Schmittbuhl, J. (2013). The long precursory phase of most large interplate earthquakes. *Nature Geosci.,* 6, 299–302. https://doi.org/10.1038/ngeo1770.

Cabrera, L., Poli, P., & Frank, W. B. (2022). Tracking the spatio-temporal evolution of foreshocks preceding the M_w 6.1 2009 L'Aquila earthquake. *Journal of Geophysical Research*: Solid Earth, 127, e2021JB023888. https://doi.org/10.1029/2021JB023888.

Carannante, S., Monachesi, G., Cattaneo, M., Amato, A., & Chiarabba, C. (2013). Deep structure and tectonics of the northern-central Apennines as seen by regional-scale tomography and 3-D located earthquakes. *J. Geophys. Res*., 118, 5391–5403. https://doi.org/10.1002/jgrb.50371.

Chen, K.H., Nadeau, R.M., & Rau, R.-J. (2008) Characteristic repeating earthquakes in an arc-continent collision boundary zone: the Chihshang fault of eastern Taiwan. *Earth Planet Sci Lett.,* 276, 262–27. https://doi.org/10.1016/j.epsl.2008.09.021.

Chiaraluce, L., Di Stefano, R., Tinti, E., Scognamiglio, L., Michele, M., Casarotti, E., Cattaneo, M., De Gori, P., Chiarabba, C., Monachesi, G., et al. (2017). The 2016 Central Italy seismic sequence: A first look at the mainshocks, aftershocks, and source models. *Seismol. Res. Lett.,* 88(3), 757–771. https://doi.org/10.1785/0220160221.

Chiodini, G., Cardellini, C., Caliro, S., Chiarabba, C., & Frondini, F. (2013). Advective heat transport associated with regional Earth degassing in central Apennine (Italy). *Earth And Planetary Science Letters*, 373, 65-74. https://doi.org/10.1016/j.epsl.2013.04.009.

Crotwell, H.P., Owens, T.J., & Ritsema, J. (1999). The TauP Toolkit: Flexible seismic travel-time and ray-path utilities. *Seismol. Res. Lett.,* 70, 154–160. https://doi.org/10.1785/gssrl.70.2.154.

Ellsworth, W.L., & Bulut, F. (2018). Nucleation of the 1999 Izmit earthquake by a triggered cascade of foreshocks. *Nat. Geosci.*, 11, 531–535. https://doi.org/10.1038/s41561-018-0145-1.

Eshelby, J.D. (1957). The determination of the elastic field of an ellipsoidal inclusion and related problems. *Proc. R. Soc. Lond. A*, 241 1226, 376-396.

INGV Seismological Data Centre. (2006, January 1). Rete Sismica Nazionale (RSN). Istituto Nazionale di Geofisica e Vulcanologia (INGV), Italy. https://doi.org/10.13127/SD/X0FXNH7QFY.

ISIDe Working Group. (2007). Italian Seismological Instrumental and Parametric Database (ISIDe). Istituto Nazionale di Geofisica e Vulcanologia (INGV). https://doi.org/10.13127/ISIDE.

ISIDE Working Group (2007). Rete Sismica Nazionale (RSN). Istituto Nazionale di Geofisica e Vulcanologia (INGV), Italy. https://doi.org/10-13127/SD/X0FXNH7QFY.

Kagan, Y. Y., & Jackson, D. D. (1991). Long-term earthquake clustering. *Geophysical Journal International*, 104(1), 117-133.

Kato, A., & Ben-Zion, Y. (2021) The generation of large earthquakes. *Nat. Rev. Earth Environ.,* 2**,** 26–39. https://doi.org/10.1038/s43017-020-00108-w.

Kato, A., Obara, K., Igarashi, T., Tsuruoka, H., Nakagawa, S., & Hirata, N. (2012). Propagation of slow slip leading up to the 2011 M_w 9.0 Tohoku-Oki earthquake. *Science,* 335(2), 705–708. https://doi.org/10.1126/science.1215141.

Krischer, L., Megies, T., Barsch, R., Beyreuther, M., Lecocq, T., Caudron, C., & Wassermann, J. (2015). ObsPy: A bridge for seismology into the scientific Python ecosystem. *Computational Science & Discovery,* 8(1), 014003. https://doi.org/10.1088/1749-4699/8/1/014003.

Lomax, A., Virieux, J., Volant, P., & Berge, C. (2000). Probabilistic earthquake location in 3D and layered models: Introduction of a Metropolis-Gibbs method and comparison with linear locations, in *Advances in Seismic Event Location* Thurber, C.H., and N. Rabinowitz (eds.), Kluwer, Amsterdam, 101-134.

Lombardi, A.M., Cocco, M., & Marzocchi, W. (2010). On the Increase of Background Seismicity Rate during the 1997–1998 Umbria-Marche, Central Italy, Sequence: Apparent Variation or Fluid-Driven Triggering? *Bull. Seism. Soc. Am.*, 100 (3): 1138–1152. doi.org/10.1785/0120090077

Liu, Y.-K., Ross, Z.E., Cochran, E.S., & Lapusta, N. (2022). A unified perspective of seismicity and fault coupling along the San Andreas Fault. *Science Advances*, 8, eabk1167. https://doi.org/10.1126/sciadv.abk1167.

Lucente, F.P., De Gori, P., Margheriti, L., Piccinini, D., Di Bona, M., Chiarabba, C., & Piana Agostinetti, N. (2010). Temporal variation of seismic velocity and anisotropy before the 2009 M_w 6.3 L'Aquila earthquake, Italy. *Geology,* 38, 1015–1018, https://doi.org/10.1130/G31463.1.

Malagnini, L., Parsons T., Munafò I., Mancini S., Segou M. & Geist E.L. (2022). Crustal Permeability Changes Observed From Seismic Attenuation: Impacts on Multi-

Mainshock Sequences. *Journal of Geophysical Research*. https://doi.org/10.1002/essoar.10510049.1

Malagnini, L., Lucente, F. P., De Gori, P., Akinci, A., & Munafò, I. (2012). Control of pore fluid pressure diffusion on fault failure mode: Insights from the 2009 L'Aquila seismic sequence. *J. Geophys. Res.,* 117, B05302. https://doi.org/10.1029/2011JB008911.

Mandler, E., Pintori, F., Gualandi, A., Anderlini, L., Serpelloni, E., & Belardinelli, M. E. (2021). Post-seismic deformation related to the 2016 Central Italy seismic sequence from GPS displacement time-series. *J. Geophys. Res.*, 126, e2021JB022200. https://doi.org/10.1029/2021JB022200.

Michele, M., Latorre, D., & Emolo, A. (2019). An Empirical Formula to Classify the Quality of Earthquake Locations. *Bull. Seism. Soc. Am.*, 109 (6): 2755–2761. https://doi.org/10.1785/0120190144.

Michele, M., Chiaraluce, L., Di Stefano,R., & Waldhauser, F. (2020). Fine-scale structure of the 2016–2017 Central Italy seismic sequence from data recorded at the Italian National Network. *Journal of Geophysical Research*: Solid Earth, 125, e2019JB018440. https://doi.org/10.1029/2019JB018440.

Munafò, I., Malagnini, L., & Chiaraluce, L. (2016). On the relationship between M_w and M_L for Small Earthquakes. *Bull. Seism. Soc. Am.,* 106, 2402–2408. https://doi.org/10.1785/0120160130.

Ogata, Y., & Katsura, K. (2012). Prospective foreshock forecast experiment during the last 17 years. *Geophys. J. Int.*, 191, 1237–1244. https://doi.org/10.1111/j.1365-246X.2012.05645.x

Poupinet, G., Ellsworth, W.L., & Frechet, J. (1984). Monitoring velocity variations in the crust using earthquake doublets: an application to California's Calaveras fault. *J. Geophys. Res.,* 89(B7), 5719–5731.

Renard, F., McBeck, J., Kandula, N., Cordonnier, B., Meakin, P., & Ben-Zion, Y. (2019). Volumetric and shear processes in crystalline rock approaching faulting. *Proceedings of the National Academy of Sciences*, 116, 16234-16239. https://doi.org/10.1073/pnas.1902994116.

Ripepe, M., Piccinini, D., & Chiaraluce, L. (2000). Foreshock sequence of september 26th, 1997 Umbria-Marche earthquakes. *Journal of Seismology*, 4(4), 387–399.

Ross, Z.E., Trugman, D.T., Hauksson, E., & Shearer, P.M., (2019). Searching for hidden earthquakes in Southern California. *Science,* 364, 767–771. https://doi.org/10.1126/science.aaw6888.

Ross, Z.E., & Cochran, E.S. (2021). Evidence for latent crustal fluid injection transients in Southern California from long-duration earthquake swarms. *Geophys. Res. Lett.,* 48, e2021GL092465. https://doi.org/10.1029/2021GL092465.

Scognamiglio, L., Tinti, E., & Quintiliani, M. (2006). Time Domain Moment Tensor (TDMT) [Data set]. Istituto Nazionale di Geofisica e Vulcanologia (INGV). https://doi.org/10.13127/TDMT.

Scognamiglio, L., Tinti, E., Casarotti, E., Pucci, S., Villani, F., Cocco, M., Magnoni, F., Michelini, A., & Dreger, D. (2018). Complex fault geometry and rupture dynamics of the M_w 6.5, 30 October 2016, central Italy earthquake. *J. Geophys. Res.*, Solid Earth, 123 (2018), 2943-2964. https://doi.org/10.1002/2018JB015603.

Shakibay Senobari, N., & Funning G.J. (2019). Widespread Fault Creep in the Northern San Francisco Bay Area Revealed by Multistation Cluster Detection of Repeating Earthquakes, *Geophys. Res. Lett.*, 46, 6425-6434. https://doi.org/10.1029/2019GL082766.

Simon, V., Kraft, T., Diehl, T., & Tormann, T. (2021). Possible precursory slow-slip to two ML~ 3 main events of the Diemtigen microearthquake sequence, Switzerland. *Geophys. Res. Lett.*, 48(19), e2021GL093783. https://doi.org/10.1029/2021GL093783.

Sugan, M., Kato, A., Miyake, H., Nakagawa, S., & Vuan, A. (2014). The preparatory phase of the 2009 M_w 6.3 L'Aquila earthquake by improving the detection capability of low-magnitude foreshocks. *Geophys. Res. Lett.*, 41, 6137–6144, https://doi.org/10.1002/2014GL061199.

Sugan, M., Vuan, A., Kato, A., Massa, M., & Amati, G. (2019). Seismic evidence of an early afterslip during the 2012 sequence in Emilia (Italy). *Geophys. Res. Lett.*, 46, 625–635. https://doi.org/10.1029/ 2018GL079617.

Sugan, M., Campanella, S., Vuan, A., & Shakibay Senobari, N. (2022). A Python Code for detecting true Repeating Earthquakes from Self-similar Waveforms (FINDRES). Accepted *Seismological Research Letters*.

Tan, Y.J., Waldhauser, F., Ellsworth, W.L., Zhang, M., Zhu, W., Michele, M., Chiaraluce, L., Beroza, G.C., & Segou, M. (2021). Machine-Learning-Based High-Resolution Earthquake Catalog Reveals How Complex Fault Structures Were Activated during the2016–2017 Central Italy Sequence. *The Seismic Record*, 1,11–19. https://doi.org/10.1785/0320210001.

Tape, C., Holtkamp, S., Silwal, V. et al. (2018). Earthquake nucleation and fault slip complexity in the lower crust of central Alaska. *Nature Geosci.,* 11**,** 536–541. https://doi.org/10.1038/s41561-018-0144-2.

Tinti, E., Scognamiglio, L., Michelini, A., & Cocco, M. (2016). Slip heterogeneity and directivity of the ML 6.0, 2016, Amatrice earthquake estimated with rapid finite-fault inversion, *Geophys. Res. Lett.*, 43, 10,745–10,752. https://doi.org/10.1002/2016GL071263.

Trippetta, F., Collettini, C., Barchi, M.R., Lupattelli, A., & Mirabella, F. (2013). A multidisciplinary study of a natural example of a CO_2 geological reservoir in central Italy, *International Journal of Greenhouse Gas Control*, 12, 72-83. https://doi.org/10.1016/j.ijggc.2012.11.010.

Uchida, N. (2019). Detection of repeating earthquakes and their application in characterizing slow fault slip. *Prog. Earth Planet Sci.,* 6, 40. https://doi.org/10.1186/s40645-019-0284-z.

Valoroso, L., Chiaraluce L., Piccinini D., Di Stefano R., Schaff D., & Waldhauser F. (2013). Radiography of a normal fault system by 64,000 high-precision earthquake locations: The 2009 L'Aquila (Central Italy) case study. *J. Geophys. Res.*, 118, 1156–1176. https://doi.org/10.1002/jgrb.50130.

Vičič, B., Aoudia, A., Borghi, A., Momeni, S., & Vuan, A. (2020). Seismicity rate changes and geodetic transients in Central Apennines. *Geophys. Res. Lett.*, 47, e2020GL090668. https://doi.org/10.1029/2020GL090668.

Vidale, J.E., & Shearer, P.M. (2006). A survey of 71 earthquake bursts across southern California: Exploring the role of pore fluid pressure fluctuations and aseismic slip as drivers. *Journal of Geophysical Research*: Solid Earth, 111, B05312. https://10.1029/2005JB004034.

Vuan, A., Sugan, M., Chiaraluce, L., & Di Stefano, R. (2017). Loading rate variations along a mid-crustal shear zone preceding the M_w 6.0 earthquake of 24 August 2016 in Central Italy. *Geophys. Res. Lett.*, 44. https://doi.org/10.1002/2017GL076223.

Vuan, A., Sugan, M., Amati, G., & Kato, A. (2018). Improving the detection of low-magnitude seismicity preceding the M_w 6.3 L'Aquila earthquake: Development of a scalable code based on the cross-correlation of template earthquakes. *Bull. Seism. Soc. Am.*, 108(1), 471–480. https://doi.org/10.1785/0120170106.

Vuan, A., Brondi, P., Sugan, M., Chiaraluce, L., Di Stefano, R., & Michele, M. (2020). Intermittent slip along the Alto Tiberina low-angle normal fault in central Italy. *Geophys. Res. Lett.,* 47, e2020GL089039. https://doi.org/ 10.1029/2020GL089039.

Waldhauser, F., Michele, M., Chiaraluce, L., Di Stefano, R., & Schaff, D. P. (2021). Fault planes, fault zone structure and detachment fragmentation resolved with high precision aftershock locations of the 2016-2017 central Italy sequence. *Geophys. Res. Lett.*, 48, e2021GL092918. https://doi.org/10.1029/2021GL092918.

Waldhauser, F., & Ellsworth, W.L. (2000). A double-difference earthquake location algorithm: Method and application to the northern Hayward Fault, California. *Bull. Seism. Soc. Am.*, 90(6), 1353–1368. https://doi.org/10.1785/0120000006.

Waldhauser, F. (2001). hypoDD: A program to compute double-difference hypocenter locations, U.S. Geol. Surv. Open File Rep., 01-113.

Wessel, P., & Luis, J.F. (2017). The GMT/MATLAB toolbox. Geochemistry, Geophysics, Geosystems, 18, 811–823. https://doi.org/10.1002/2016GC006723.

Zaliapin, I., & Ben-Zion, Y. (2020). Earthquake declustering using the nearest-neighbor approach in the space-time-magnitude domain. *J. Geophys. Res.*, 125, e2018JB017120. https://doi.org/10.1029/2018JB017120.

Zaliapin, I., & Ben-Zion, Y. (2016). A global classification and characterization of earthquake clusters. *Geophys. J. Int.*, 207, 608–634. https://doi.org/10.1093/gji/ggw300.

Zhu, W., Allison, K.L., Dunham, E.M., & Yang, Y. (2020). Fault valving and pore pressure evolution in simulations of earthquake sequences and aseismic slip. *Nat Commun.*, 11, 4833. https://doi.org/10.1038/s41467-020-18598-z.

Figures

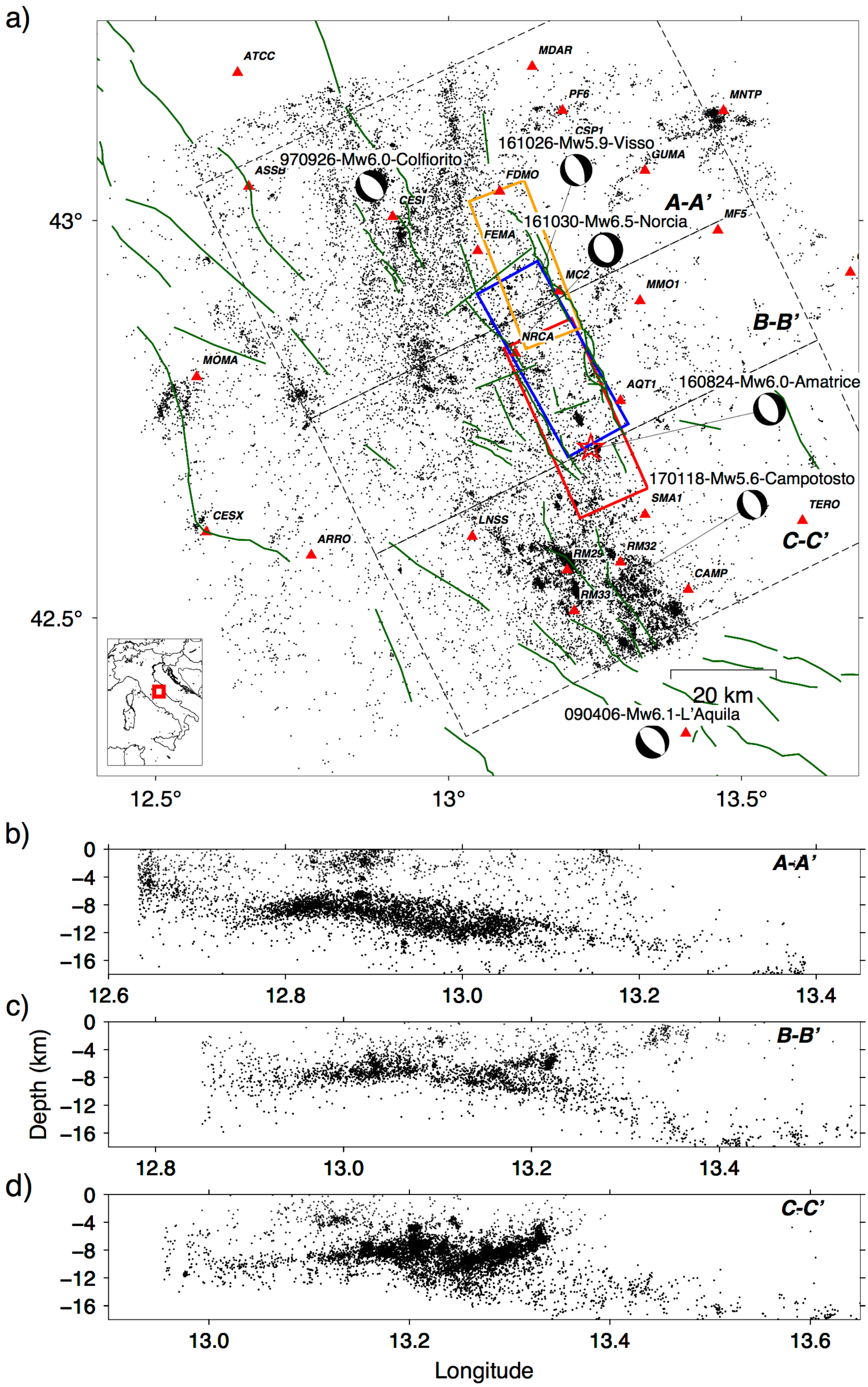

Figure 1 – a) Map showing the selected templates (black dots) and stations (red triangles) used in the template matching analysis. Faults are projected at the surface

as boxes: Amatrice (red, Tinti et al., 2016), Visso (orange, Chiaraluce et al., 2017), Norcia (blue, Scognamiglio 2018). The red star marks the 24th August Amatrice epicenter. Green lines show normal faults (Barchi et al., 2021). Focal mechanisms from Scognamiglio et al., 2006. b) A-A', c) B-B', d) C-C' along dip cross-sections of seismicity from 2009 to 2016 (24th August), where is apparent the almost flat shear zone in the middle crust.

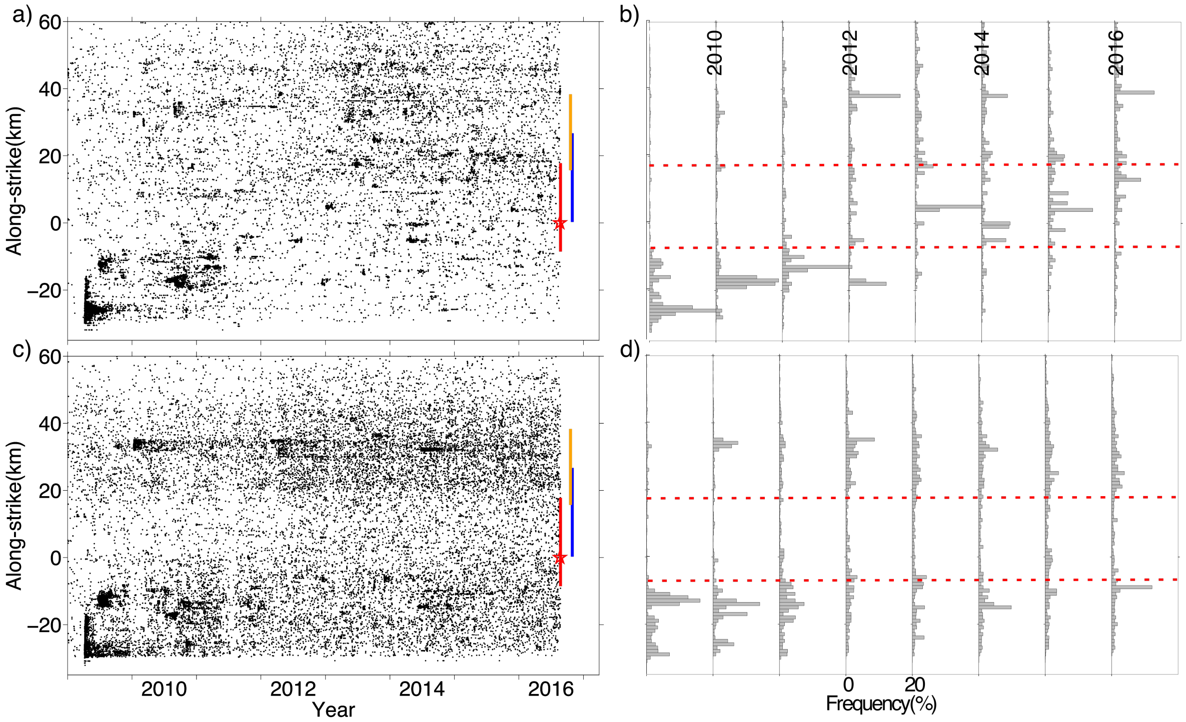

Figure 2 – a) Spatiotemporal distribution of the augmented catalog in the shallow crust above the TSZ and b) the corresponding yearly frequency of events projected along the main fault strike (336 degrees). Only events with M>=Mc are plotted. c) and d) panels as a) and b) for events below the TZS. Red dotted lines represent the northern and southern edges of the 24th August M_w 6.0 Amatrice main fault. Faults are projected at the surface for the Amatrice mainshock (red), Visso (orange), and Norcia (blue). The red star marks the 24th August Amatrice epicenter.

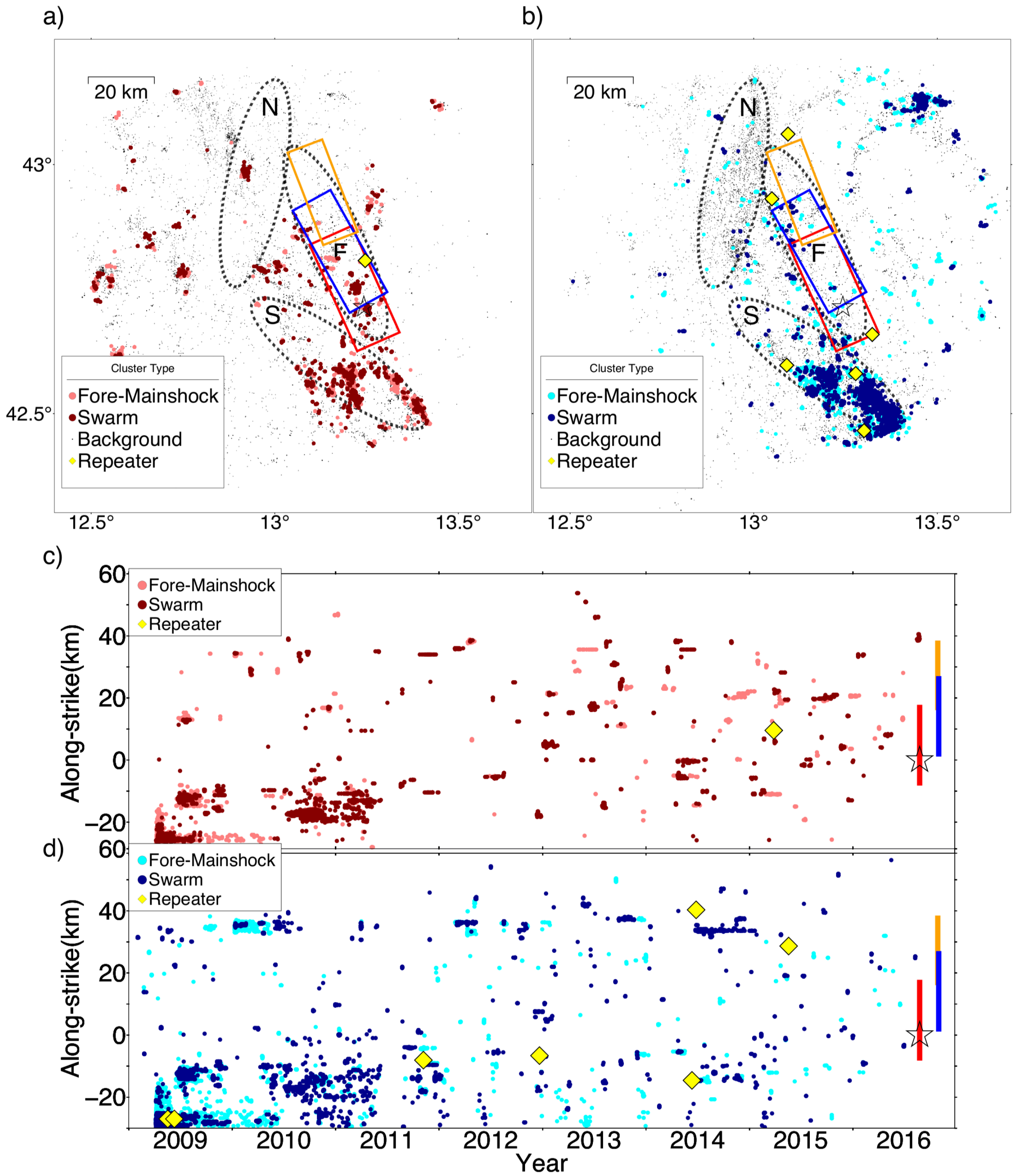

Figure 3 – a) Map showing swarm-like, foreshock-mainshock clusters, and background seismicity above the SZ, b) as a) below the top of SZ. Only clusters with at least 10 events are shown. Yellow diamonds show the repeating earthquakes, identified using a 0.97 cross-correlation value (supplementary **Text S4**). Dashed black lines identify the faults regions (F), the southern regions (S), where clusters

prevail, and the northern region (N), where background seismicity prevails. c) along-strike section of the clusters above SZ and d) below the top of SZ. Faults are projected for the Amatrice mainshock (red), Visso (orange), and Norcia (blue); the white star marks the position of the 24th Amatrice mainshock.

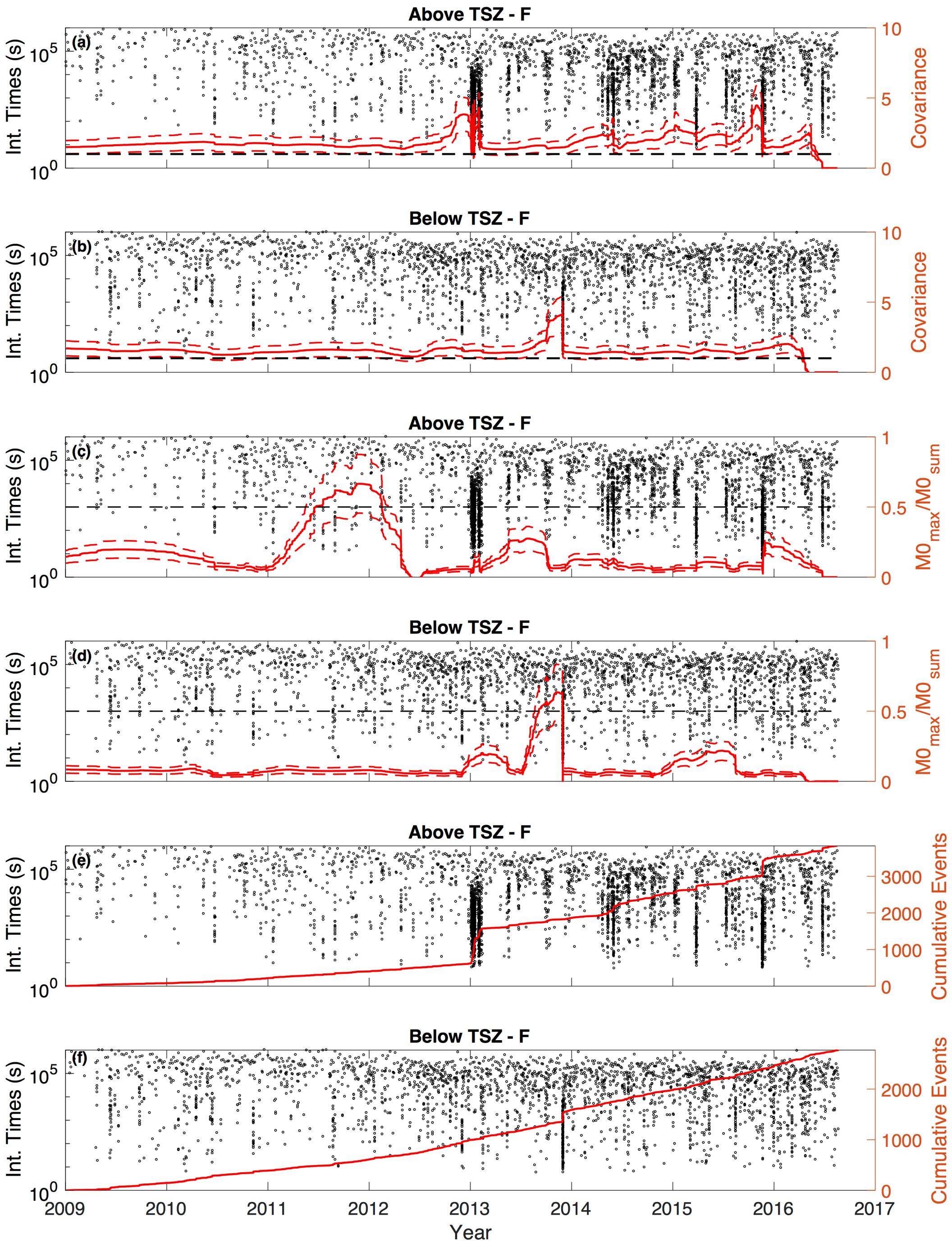

Figure 4 – Covariance values of interevent times above (a) and below (b) the TSZ. Moment ratio of interevent times above (c) and below (d) the TSZ. Dashed lines show the associated standard deviation. The cumulative number of events above (e) and below (f) the TSZ is also shown. The analysis is performed for the fault volume (F in Figures 3a and b).